Micro-Void Toughening of Thermosets and Its Mechanism

Nam Ho Kim, Ho Sung Kim

Mechanical Engineering, School of Engineering, Faculty of Engineering and Built Environment, University of Newcastle, Callaghan NSW 2308, Australia

Received 15 June 2004; accepted 4 February 2005
DOI 10.1002/app.22262
Published online in Wiley InterScience (www.interscience.wiley.com).

ABSTRACT: Void toughening is studied using epoxy resin. Voids were produced mechanically without any chemical agents so that it was possible to isolate the role of micro-voids from other factors. Toughness of the epoxy resin owing to voids was improved over that of the control by an order of magnitude. The toughening mechanism was found to be strongly related to intervoid distance and, hence, to void-to-crack distance. Large deformation bands between the crack and voids were deduced to be the source of toughening. The intervoid distance was directly measured on scanning electron microscope photos. © 2005 Wiley Periodicals, Inc. J Appl Polym Sci 98: 1290–1295, 2005

Key words: cavitation; fracture toughness; inter-void distance; shear deformation; toughening; void

INTRODUCTION

Toughening of thermosets, such as epoxies, has been achieved by the addition of second phase particles.[1–4] Toughening mechanisms include: (a) localized shear band formation between rubber particles,[5] (b) cavitation of rubber particles or matrix,[5] and (c) bridging of rubber particles.[6] Huang and coworkers[7] have suggested that the first two mechanisms, unlike the last one, do not require the rubber particles to be well bonded to the matrix. Thus, a question arises—how would thermosets without rubber particles but containing micro-voids behave? Waddill[8] has suggested a way, involving chemical agents, of preparing epoxy systems containing micro-voids and proposed that such materials may exhibit an improved toughness. Huang and Kinloch[9] investigated toughening of epoxies containing micro-voids produced in the way suggested by Waddill[8] and confirmed the fracture toughness increases due to the presence of micro-voids. Also, they deduced from the change of yield stress and fracture strain that the voided epoxy can more easily undergo plastic deformation than the control material and found that the cavitation of voids occurred. Bagheri and Pearson[10] also investigated the toughening of epoxies due to micro-voids, using hollow latex particles. They discussed the influence of the shell of the hollow latex for the resulting improved fracture toughness. The micro-voids used in studies by previous researchers, thus, were either produced by chemical agents or surrounded by materials different from those of the matrix.

In this study, a technique was developed to produce micro-voids without chemical agents so that it was possible to isolate the role of micro-voids from other factors. Also, toughening mechanisms associated with micro-voids are presented.

EXPERIMENTAL

Materials

Epoxy 105 was used as a model material for study. It is a blend of Bisphenol A and Bisphenol F and is produced by West System. The curing agent used was a Slow Hardener 206 (aliphatic amines and aliphatic amine adducts based on diethylene triamine, and triethylene triamine).

Preparation for specimens of micro-voids

Micro-voids in the epoxy system were produced by vigorous stirring using a mechanical overhead stirrer (IKA, RW 20 n with a 4-bladed propeller, each blade with the dimension of 25 × 8 × 1 mm) according to the following procedure. A predetermined amount of epoxy was placed in a 200 mL beaker (with a diameter of 90mm and a height of 120mm) and then 17phr (by weight) of curing agent was added. The mixture was stirred for 5 min for various stirrer speeds ranging from 400 to 1700 rpm measured using a hand tachometer, TM-2011, Dynapar, and then poured into an aluminum mold and placed in an oven for about 5 min preheating at 135°C. Further, the mold was left in the oven at 135°C for 2 h curing and then was removed

Correspondence to: H. S. Kim (ho-sung.kim@newcastle.edu.au).

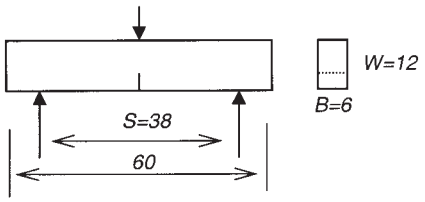

Figure 1 Three-point loading for both flexural and fracture tests but without the notch for flexural tests.

from the oven to allow it to cool gradually and left for at least one day at room temperature. Thus, eleven different types, depending on stirring speed, of epoxy systems containing micro-voids were prepared. For micro-void characterization, scanning electron microscopic (SEM) photos for the fracture surface area of 6.5 × 2 mm close to the initial crack were used for measurements of volume fractions, two dimensional diameters, and numbers.

Mechanical testing

All the specimens for mechanical testing were machined into dimensions of 12 × 60 × 6 mm for edgewise placement, as shown in Figure 1. Three point bending tests on a universal testing machine (Shimadzu 5000) were conducted for elastic modulus, strength, and fracture toughness. A crosshead speed of 10 mm/min was adopted for tests of flexural properties and 0.5 mm/min for the fracture toughness measurements at a room temperature of 21°C.

Elastic moduli (E) and flexural strengths (σ_y) were calculated using the following equations given in ASTM D 970M –93:

$$E = \frac{S^3 m}{4BW^3} \tag{1}$$

and

$$\sigma_y = \frac{3PS}{2BW^2} \tag{2}$$

where S is the support span, B is the thickness, W is the width, m is the slope of the tangent to the initial straight-line portion of the load-deflection curve, and P is the load.

The critical stress intensity factor (K_{IC}) expression[11] used was

$$K_{IC} = \frac{3PS\sqrt{\pi a}}{2BW^2} Y \tag{3}$$

where a is the crack length and Y is a geometry factor given by

$$Y = \frac{1}{\sqrt{\pi}} \frac{1.99 - \frac{a}{W}\left(1 - \frac{a}{W}\right)\left(2.15 - 3.93\frac{a}{W} + 2.7\left(\frac{a}{W}\right)^2\right)}{\left(1 + 2\frac{a}{W}\right)\left(1 - \frac{a}{W}\right)^{3/2}}. \tag{4}$$

A precrack, 4 to 5 mm long, was produced by tapping a razor blade into the tip of a saw-cut notch, 2mm long, of each fracture test specimen, and its length was measured with a pair of Vernier calipers.

Specific fracture energy values for mode I were approximated using

$$G_{IC} = \frac{K_{IC}^2}{E}. \tag{5}$$

Microscopy

SEM work using an Oxford-XL30 Philips was conducted for specimens coated with gold. The specimens were cleaned with water using a Bran Sonic 52 and dried in an oven at 30°C for 30 min before coating for SEM.

Thin sections taken from the mid-plane of test specimens were prepared for transmission microscopy (Axioplan 2, Carl Zeiss). The thicknesses of the thin sections obtained were about 19μm. Two different types of thin section specimens were prepared—one is from the usual single cracked specimens described above and the other is from double U-notch four point bending (DN-4PB) specimens already described elsewhere.[12] The DN-4PB specimens were to provide supportive evidence for deformation. The DN-4PB specimens were loaded at a crosshead speed of 0.5 mm/min until one of the notches fractured and the other surviving notch was used for thin sectioning. The radius of the U-notch was 1mm.

Intervoid distance measurement

Intervoid distance was directly measured using an image analyzer (Scion Image) after drawing digital lines on SEM computer images. The following triangulation procedure was adopted to draw lines between voids (more details are given elsewhere[13]):

1. Nominate an arbitrary void for commencement.
2. Choose a nearest void to the first nominated void and then draw a connecting line between the two surfaces of voids.
3. Choose another void that is the nearest to the midpoint between the previous two void surfaces.

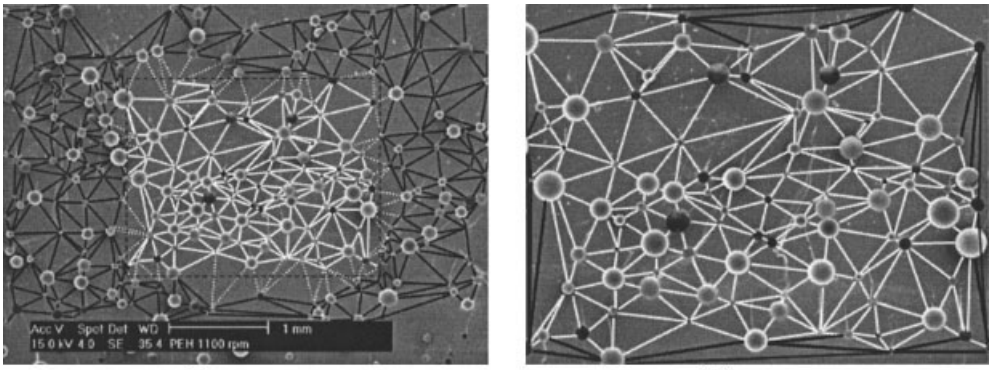

Figure 2 An example of triangulation for intervoid distance measurement: (a) after removing lines affected by the "edge effect," where white dotted lines are affected by the edges when the middle section of the black dashed line is taken as an image for measurement; and (b) image taken from (a) where black lines along the edges of the image are fictitious as compared with the white dotted line in (a).

4. Draw a triangle connecting the previous two void surfaces.
5. Repeat steps 3 and 4 using one of the unused and outermost lines of triangles until all the voids are connected.
6. Remove all the lines affected along the edges of the triangulation network. Finally, measure intervoid distance.

An example for lines affected by the edges of the triangulation network (see step 6 above) is given in Figure 2.

RESULTS AND DISCUSSION

Micro-voids produced in the epoxy system were characterized as a function of stirrer rpm, as shown in Figure 3. Void fraction (Fig. 3a) appears to increase abruptly at around 900 rpm and then reached a high value at 1400 rpm but decreased thereafter. Average void size (Fig. 3b) is more or less independent of stirring speed, although some significant scatter is noticed. The number of voids (Fig. 3c), however, generally increases with stirring speed. The intervoid distance (Fig. 3d) appears to decrease down to 1400 rpm and then slightly increase for 1500 rpm and 1700 rpm, which were found to not contribute much to toughening.

Elastic modulus and flexural strength were plotted with the least squared lines as functions of volume fraction of voids in Figures 4 and 5, respectively. Both properties are seen to be well correlated with the volume fraction of voids, as correlation coefficients were found to be -0.94 and -0.89 for elastic modulus and flexural strength, respectively. As expected, reduction in properties occurs as the volume fraction increases.

Specific fracture energy (G_{IC}) is plotted as a function of volume fraction of voids in Figure 6. It appears that there is a sudden increase in G_{IC} around a volume fraction of 0.12. It is highlighted that the maximum increase represents about 11 times that of the control. SEM fracture surface images were examined and it was found that they generally reflect the trend appearing in Figure 6. Specimens of high toughness (1200 rpm and 1400 rpm), as shown in Figure 7, tend to posses rough fracture surfaces. Also, they are seen to have nucleation sites for crack propagation on fracture surfaces. This indicates that the crack propagation of specimens with high fracture toughness is not of continuous forward movement, but fracture energy is accumulated and then released suddenly. One can speculate that such resistance to cracking at initiation would be caused by a blunting effect due to the presence of relatively large void sizes in the vicinity of the initial crack tip. However, this speculation is not supported by the fact that, for similar volume fractions of voids (Fig. 3a), fracture toughness values of specimens prepared at 1000 rpm, 1100 rpm, 1500 rpm, and 1700 rpm are low (not toughened) compared to those (toughened) at 1200 rpm and 1300 rpm despite their similar or higher void diameters (Fig. 3b) compared to those of 1200 rpm and 1300 rpm.

Further, to gain an insight into the microscopic deformation influenced by voids, G_{IC} as a function of intervoid distance is also plotted in Figure 8. The intervoid distance is an important parameter for plane-stress/strain transition at microscopic scale, as first suggested by Wu[14]—if the intervoid distance is smaller than a critical value, plane stress deformation requiring large energy would occur and vice versa. A transition appears to occur at around 140μm of inter-

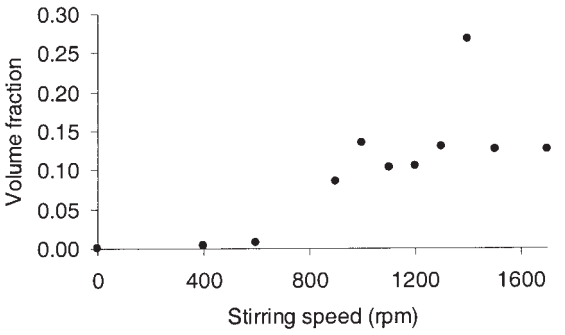

(a)

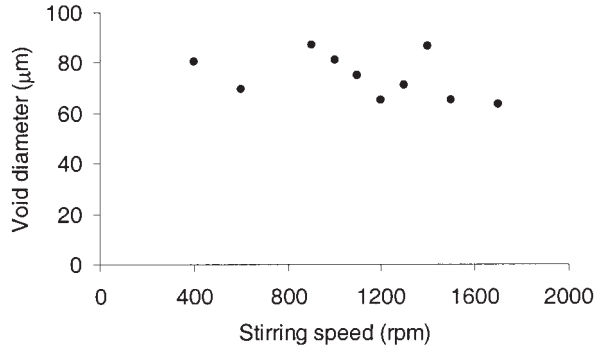

(b)

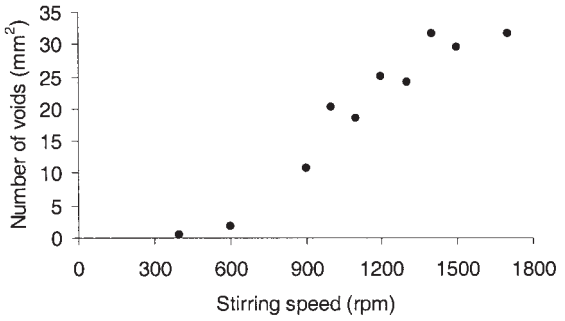

(c)

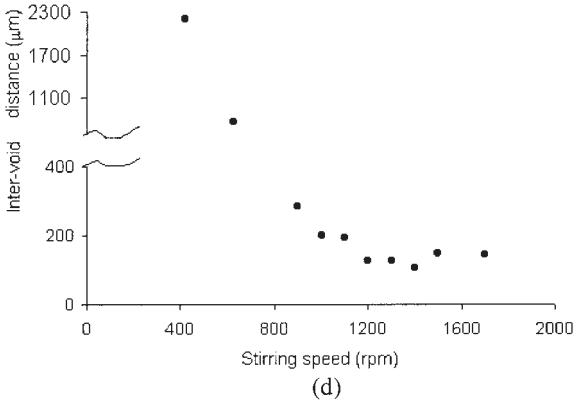

(d)

Figure 3 Void formation influenced by stirring speed: (a) volume fraction, (b) void diameter, (c) void number, and (d) intervoid distance.

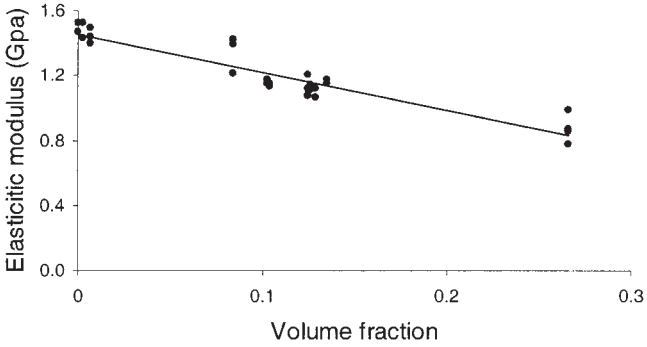

Figure 4 Flexural modulus of epoxy systems versus void volume fraction. Correlation coefficient was found to be −0.94.

void distance (Fig. 8). This leads to a hypothesis that the transition coincides with a microscopic plane stress/strain transition.

To test the hypothesis, deformation around a crack tip of a specimen prepared at 1400 rpm was examined by thin sectioning, as shown in Figure 9. Figure 9a shows a polarized image of voids and a crack prepared using a once-loaded specimen. Figure 9b is the same thin section but without polarization, to see the location of the crack. In the polarized image, some

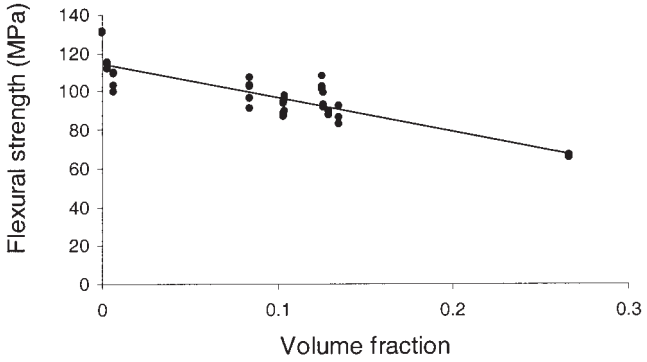

Figure 5 Flexural strength of epoxy systems versus void volume fraction. Correlation coefficient was found to be −0.89.

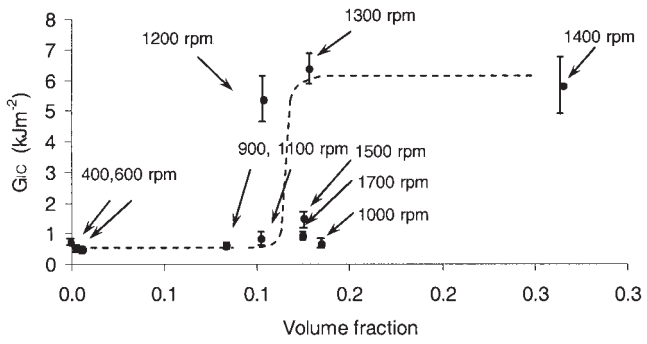

Figure 6 Specific fracture energy (G_{IC}) versus void volume fraction for epoxy systems.

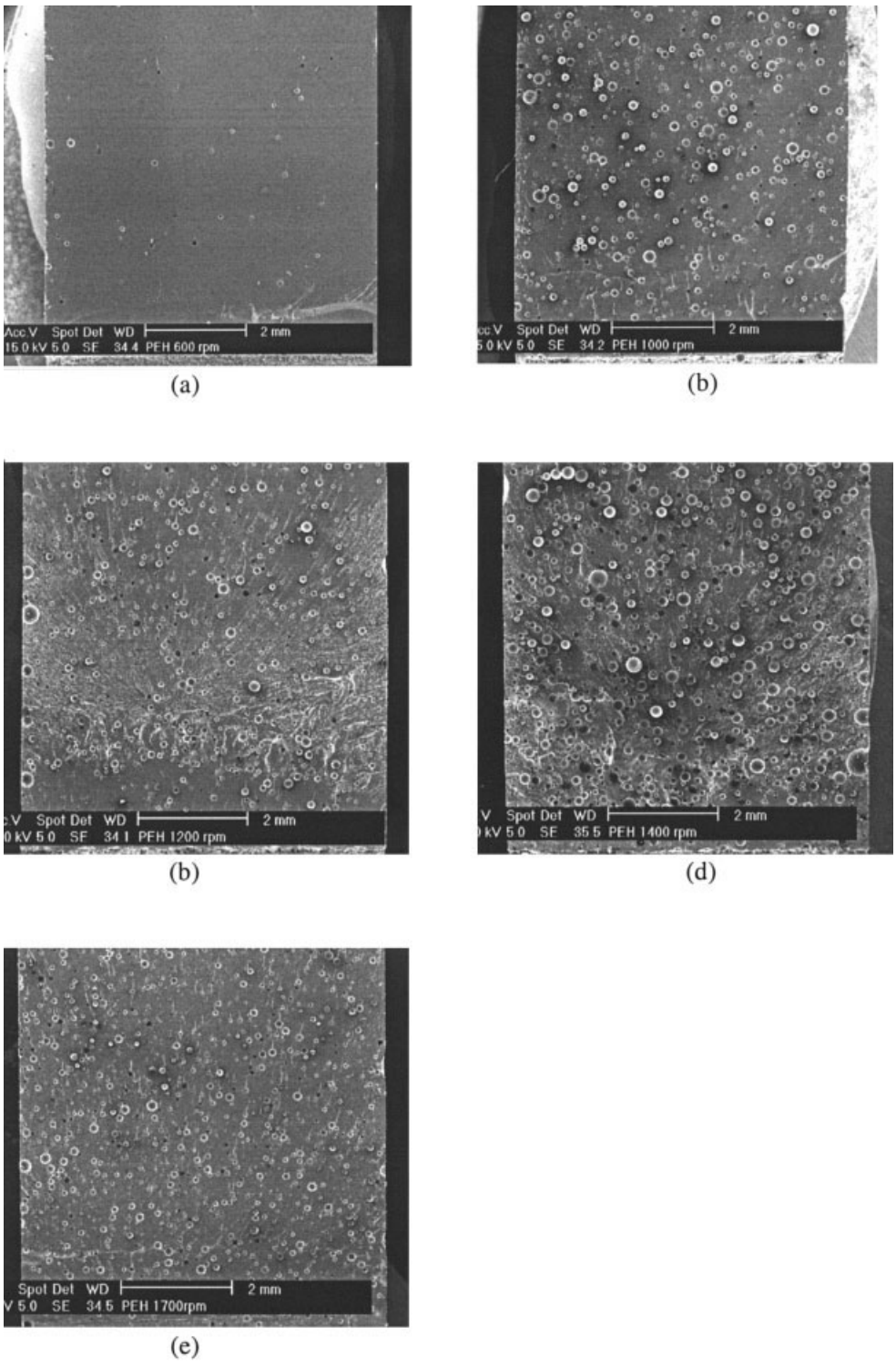

Figure 7 SEM fracture surface images in the vicinity of the precrack: (a) 600rpm, (b) 1000rpm, (c) 1200rpm, (d) 1400rpm, and (e) 1700rpm. Crack propagation direction is bottom to top.

weak fringe patterns are seen around the voids, indicating some residual stress exists, perhaps due to shrinkage during curing.[15] More importantly, deformation bands connecting between the crack and voids along the crack path are seen. This appearance is different from those in the literature,[12,16] where connecting bands are more between voids than between the crack and voids. The reason for this appears to be that, when void size and intervoid distance are as large as those in the present case, not many voids are

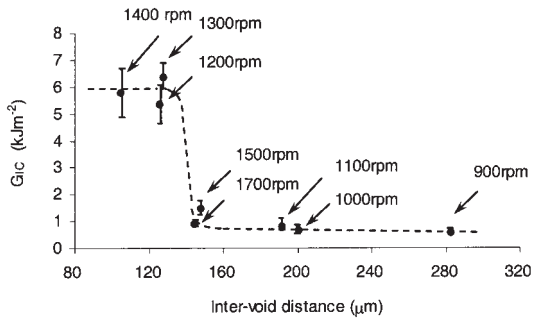

Figure 8 Specific fracture energy (G_{IC}) versus intervoid distance for epoxy systems. Data points for 400 rpm (intervoid distance and G_{IC} are 2194 μm and 0.47 kJm^{-2}, respectively) and 600 rpm (intervoid distance and G_{IC} are 768 μm and 0.45 kJm^{-2}, respectively) are not plotted because they are out of scale.

within the process zone but larger deformation bands are possible. Thus, the intervoid distance provides a good correlation with void-crack distance; maximum crack-to-void distance is about half the intervoid distance. The voids thus play a role in production of deformation bands. This is further supported by images shown in Figure 10. The polarized image (Fig. 10a) obtained from the DN-4PB test and thin sectioning show deformation bands connecting between voids. Figure 10b is the same thin section as Figure 10a, but without polarization so that locations of voids are well seen. Consequently, the hypothesis that the transition between high and low fracture toughness coincides with a microscopic plane stress/strain transition is supported.

In addition, void sizes on fracture surfaces, both near (slow cracking) and far (fast cracking) from the initial crack of toughened epoxies were examined, but no sign of cavitation was found.

CONCLUSIONS

Void toughening for epoxy resin has been successfully achieved without chemical agents. The toughening mechanisms involved have been discussed, and it was deduced that toughening is mainly due to shear bands between voids and a crack.

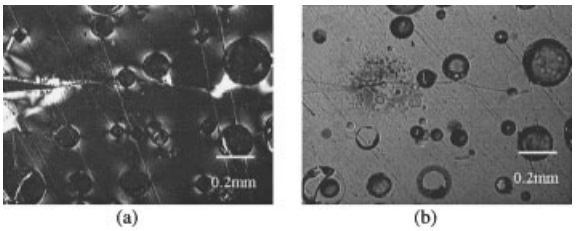

Figure 9 Thin section for a specimen prepared at 1400 rpm for transmission microscopy: (a) cross-polarized image showing deformation bands along the crack path advanced from left to right; and (b) same section as (a) but without polarization. Some slant lines are scratches.

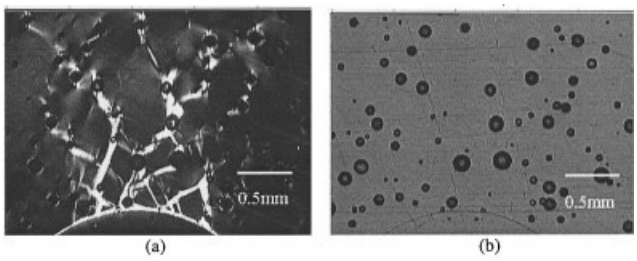

Figure 10 Thin section of double U-notch specimen prepared at 1200 rpm for transmission microscopy: (a) cross-polarized image showing deformation bands connecting between voids; and (b) same section as (a) but without polarization. U-notch is located at the bottom.

One of the authors (NHK) acknowledges the UNRS scholarship of the University of Newcastle.

References

1. Pearson, R. A.; Yee, A. F. Polymer 1993, 34, 3658.
2. Garg, A. C.; Mai, Y.-W Compos Sci Technol 1988, 31, 179.
3. Huan, Y.; Hunston, D. L.; Kinloch, A. J.; Riew, C. K. In Toughened Plastics I: Science and Engineering, Adv in Chemistry Series 233; Riew, C. K.; Kinloch, A. J., Eds.; American Chemical Society: Washington, DC, 1993; pp 1–35.
4. Kim, H. S.; Ma, P. J Appl Polym Sci 1998, 69, 405.
5. Pearson, R. A.; Yee, A. F. J Mater Sci 1986, 21, 2475.
6. Kunz-Douglass, S.; Beaumont, P. W. R.; Ashby, M. F. J Mater Sci 1980, 15, 1109.
7. Huang, Y.; Kinloch, A. J.; Bertsch, R. J.; Siebert, A. R. In Toughened Plastics I: Science and Engineering, Adv in Chemistry Series 233; Riew, C. K.; Kinloch, A. J., Eds.; American Chemical Society: Washington, DC, 1993; pp 189–210.
8. Waddil, H. G. Epoxy Adhesive Formulations with Enhanced Properties, 11th National SAMPE Technical Conference, November 13–15, 1979, pp 282–294.
9. Huang, Y.; Kinloch, A. J. Polymer 1992, 92, 1330.
10. Bagheri, R.; Pearson, R. A. Polymer 1995, 36, 4883.
11. Tada, H.; Paris, P. C.; Irwin, G. R. The Stress Analysis of Cracks Handbook; Paris Productions Incorporated: St Louis, 1985; 2nd ed, p 2.16.
12. Oh, B. S.; Kim, H. S.; Ma, P. In Toughened Plastics II: Novel Approaches in Science and Engineering; Riew, C. K.; Kinloch, A. J., Eds.; American Chemical Society: Washington, DC, 1996; Chap 8, pp 111–118.
13. Kim, N. H.; Kim, H. S. Scripta Materialia 2005, 52, 739.
14. Wu, S. J Appl Polym Sci 1988, 35, 549.
15. Lee, H.; Neville, K. Handbook of Epoxy Resins; McGraw-Hill: New York, San Francisco, Toronto, London, Sydney, 1967; p 17–11.
16. Pearson, R. A.; Yee, A. F. J Mater Sci 1989, 24, 2571.